Int. J. Heat Mass Transfer. Vol. 17, pp. 1527–1548. Pergamon Press 1974. Printed in Great Britain

THERMAL DROPLET SIZE MEASUREMENTS USING A THERMOCOUPLE

C. A. A. VAN PAASSEN
Thermal Power Laboratory of the Delft University of Technology, Delft, The Netherlands

(*Received* 28 *January* 1974)

Abstract—During the investigation on atomization and evaporation of water in steam spray coolers a thermal measuring device has been developed for droplet size measurement. This device consists of a thermocouple on which the droplet evaporates by heat removal from the thermocouple material near the hot junction; it is called: droplet detecting thermocouple (d.d.t.). The principle of a d.d.t. is based on utilization of the correlation between droplet radius and temperature signal of the d.d.t., caused by the evaporating droplet. The d.d.t. proved to be a dependable device for continuous detecting and measurement of water droplets both in air and steam flows, even at high pressures and temperatures. In this paper a theoretical analysis of the d.d.t. behaviour is given together with experimental data of d.d.ts. for water droplets with radii between 3 and 1188 μm. Good agreement between experimental data and theoretically predicted results has been reached.

NOMENCLATURE

A, area;
c, specific heat;
$\bar{c}_{dl}$, mean specific heat of droplet liquid;
$\bar{c}_{dv}$, mean specific heat of droplet vapour;
C_c, coefficient defined in equation (9);
C_{ch}, coefficient defined in equation (40);
C_t, time constant (to reach 63 per cent of the ΔT);
D, diameter;
D_{ch}, outside diameter of a sheathed thermocouple;
H, specific heat of evaporation;
k, thermal conductivity;
q, heat flux;
Q, quantity of heat;
r, droplet radius;
r_j, droplet radius obtained from equation (8) or (39) using $\theta_{0\tau} = \theta_c$ and $\tau = \tau_c$;
r_{mi}, droplet radius observed under the microscope;
r_w, real droplet radius;
Δr_e, droplet radius decrease by evaporation before microscopic observation;
t, time;
T, temperature;
T_0, initial d.d.t. temperature;
T_m, time averaged d.d.t. temperature;
ΔT, driving temperature difference;
u, impact velocity;
W_e, Weber number defined in equation (14);
x, distance.

Greek symbols

α, heat-transfer coefficient;
β, D_f/r ratio;
γ, angle;
θ, temperature drop;
θ_c, measured temperature drop (see Fig. 2);
θ_{xt}, temperature drop at distance x and time t;
κ, thermal diffusivity;
π, 3·141...;
ρ, density;
σ, surface tension;
τ, evaporation time of a droplet;
τ_c, measured cooling time (see Fig. 2);
ψ_n, correction factor, $n = 4, 5, \ldots 11$;
ψ_R, combined correction factor defined in equation (11);
ψ_w, calibration factor defined in equation (10).

Subscripts

a, thermocouple wire a;
b, thermocouple wire b;
c, thermocouple;
ch, sheathed thermocouple;
d, droplet;
e, evaporation;
f, droplet film;
h, sheath;
in, insulation;
s, saturation;
v, vapour;
∞, surroundings.

1. GENERAL ASPECTS OF THE METHOD AND MOTIVATION

THE PROBLEM of measuring the size of droplets has been encountered in different branches of engineering sciences and many different methods have been employed (Giffen and Muraszew [1]). However, the application of these methods to measurements of droplets in spray coolers raises certain difficulties:

1. The great number of droplets.
2. The relatively high and varying droplet velocity.
3. The great variation in droplet size.
4. The change in droplet size with time due to evaporation.
5. The high pressure and temperature.

All these factors limit the number of methods which can be used for measuring droplets in spray coolers. During the last few years a new method has been developed. This new method is based on measuring the temperature signal of a fast responding thermocouple due to the heat removal (mainly evaporation) by a droplet colliding with the thermocouple in the neighbourhood of the hot junction.

The measuring device has been named droplet detecting thermocouple (d.d.t.). This device has a number of advantages in overcoming the aforementioned difficulties.

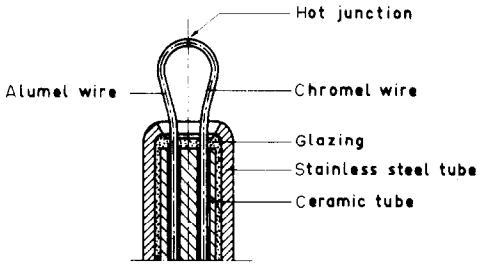

FIG. 1. Bare d.d.t.

The principle of a d.d.t. (Fig. 1) can be summarized as follows. As a droplet collides with the hot junction of the thermocouple it removes heat from it. The droplet evaporates.

In the meantime the temperature of the hot junction drops. A typical signal of a d.d.t. is shown in Fig. 2 (signal starting point at A). In Fig. 2 the part of the signal beyond point B shows reheating of the hot junction mainly due to conduction of heat from the wires of the thermocouple to the hot junction.

It is to be noted that during the entire period of the signal a secondary rise in the temperature of the thermocouple is caused by heat flow from the surroundings. In case of continuous droplet detection this heating up from the surroundings (relatively slow compared to the cooling during evaporation) assures a good time averaged d.d.t. temperature. With the aid of a simplified model and the general heat conduction theory a correlation has been derived relating the d.d.t. signal (the temperature drop θ_c and the cooling time τ_c) to the properties and dimensions of the droplet and the d.d.t.

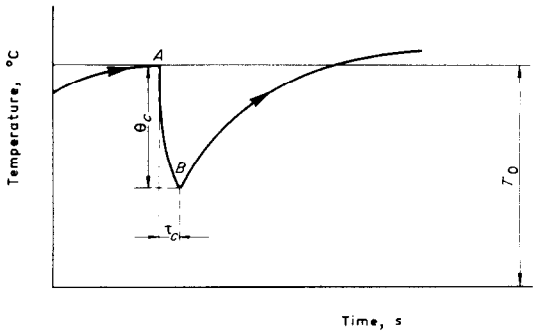

FIG. 2. Typical d.d.t. signal.

2. ANALYSIS OF d.d.t. RESPONSE

The simple model shown in Fig. 3 is adopted for computing of the temperature drop $\theta_{0\tau}$ (at $x = 0$ and $t = \tau$) due to the evaporation of a droplet at the hot junction of a d.d.t.

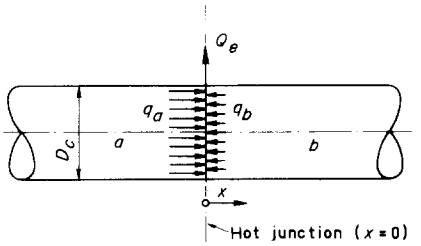

FIG. 3. Schematization of d.d.t. for heat flow analysis.

In the analysis the following assumptions are made:

1. The droplet is at saturation temperature T_s at the moment of impact.
2. The vapour leaving the droplet is not superheated by heat from the d.d.t.
3. The droplet stays attached to the d.d.t. until it evaporates completely.
4. While the droplet is attached to the d.d.t. it only receives heat from the d.d.t. and not from the other surroundings.
5. The heat flow from the d.d.t. to the droplet film is constant during the evaporation time τ.
6. The two wires a and b will both be treated as infinite slabs, in which heat flows only in the axial direction by conduction, subject to the boundary condition: heat flux q is constant at $x = 0$.

7. The properties of the wires: ρ_a, ρ_b (the density), k_a, k_b (the thermal conductivity), c_a, c_b (the specific heat) are constant.
8. Prior to the impact of the droplet on the d.d.t. (at the time $t = 0$) wires a and b are both at a constant initial temperature T_0 independent of the x distance along the axes of wires (see Fig. 3).

The solution of the heat-conduction problem for the semi-infinite slab subject to the initial and boundary conditions described above (Carslaw and Jaeger [2]) would yield for $x = 0$ and $t = \tau$:

$$\theta_{0\tau} = \frac{2q}{k}\sqrt{\left(\frac{\kappa\tau}{\pi}\right)} \tag{1}$$

where

$$\kappa = \frac{k}{\rho c}. \tag{2}$$

Equation (1) is valid for both wires (a and b). For the hot junction, i.e. $x = 0$, the left and right hand temperatures are equal:

$$\theta_a = \theta_b \quad (x = 0). \tag{3}$$

The total heat flux q_c in the hot junction is given by

$$q_c = q_a + q_b \quad (x = 0). \tag{4}$$

Substitution from (1) to (3) into (4) gives

$$\theta_{0\tau} = \frac{2q_c}{\sqrt{(\pi/\tau)}[\sqrt{(k_a\rho_a c_a)} + \sqrt{(k_b\rho_b c_b)}]}. \tag{5}$$

The heat of evaporation Q_e of a droplet with radius r, density ρ_{ds} and specific heat of evaporation (latent heat) H may be written as

$$Q_e = \frac{4}{3}\pi r^3 \rho_{ds} H. \tag{6}$$

The total heat flux q_c during the evaporation time τ at the hot junction of a thermocouple with diameter D_c is given by

$$q_c = \frac{Q_e}{(\pi/4)D_c^2\tau}. \tag{7}$$

From equations (5)–(7)

$$r^3 = C_c\theta_{0\tau}\sqrt{\tau} \tag{8}$$

denoting C_c (with dimensions $[\mathrm{m^3\,{}^\circ C^{-1}\,s^{-1/2}}]$) as a coefficient

$$C_c = \frac{3(\sqrt{\pi})D_c^2[\sqrt{(k_a\rho_a c_a)} + \sqrt{(k_b\rho_b c_b)}]}{32H\rho_{ds}}. \tag{9}$$

The value of the d.d.t. material factor $[\sqrt{(k_a\rho_a c_a)} + \sqrt{(k_b\rho_b c_b)}]$ depends on the material temperature.

This dependence is shown in Fig. 4 for the chromel–alumel combination (using Hoskins catalogue [3]).

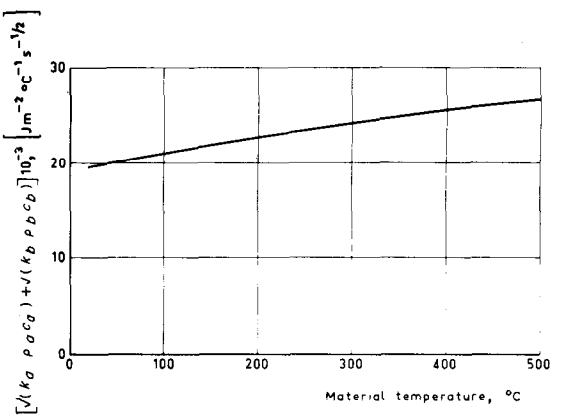

FIG. 4. Material factor $[\sqrt{(k_a\rho_a c_a)} + \sqrt{(k_b\rho_b c_b)}]$ of bare chromel–alumel d.d.t.

Because of lack of data for the change of c with temperature for chromel–alumel, the per cent changes were approximated as being the same as for pure nickel [4].

The next section will present an evaluation of the different assumptions on the d.d.t. response.

3. ESTIMATION OF CORRECTION FACTORS

In practice the basic assumptions of Section 2 are not fully realized. For this reason a calibration factor ψ_w is introduced

$$\psi_w = \frac{r_j}{r_w} \tag{10}$$

where r_j is the droplet radius calculated from equation (8) or (39) using the measured cooling time τ_c and measured temperature drop θ_c (instead of τ and $\theta_{0\tau}$) resulting in $r_j^3 = C_c\theta_c\sqrt{\tau_c}$ or $r_j^3 = C_{ch}\theta_c\sqrt{\tau_c}$, while r_w is the real droplet radius found using another measuring technique (e.g. photographic, weighing). Some data of ψ_w will be presented in Section 4. However, it is often difficult to measure the real droplet radius using another technique. For this reason an evaluation of the deviations that could result from the difference between the actual conditions and those assumed in the analysis of Section 2 is of great value. This is achieved by considering the deviations from the assumptions separately, each giving an individual correction factor ψ_n.

The combined correction factor ψ_R is then calculated using:

$$\psi_R = \psi_4\psi_5\psi_6\psi_7\psi_8\psi_9\psi_{10}\psi_{11}. \tag{11}$$

In equation (11) ψ_4 to ψ_{11} are individual correction factors due to a deviation from one or more particular assumptions. The values of the subscripts 4–11 are chosen to be consistent with the nomenclature of [5].

It turns out that ψ_R is approximately equal to ψ_w as can be seen from the experimental data found in Section 4. Using $\psi_w = \psi_R$, the droplet radius can be calculated using equations (8)–(11) without calibration measurements if the individual correction factors are determinable. The individual correction factors will be evaluated in the following sections.

3.1. *Correction factor ψ_4 due to subcooling and superheating of droplets*

If the droplet temperature T_d at the moment of impingement is below the saturation temperature T_s an extra amount of heat flowing from the d.d.t. is used to raise the droplet temperature to saturation. On the other hand the vapour leaving the droplet film may be superheated to a temperature T_v by heat removal from the d.d.t. This superheating temperature T_v is unknown but has a value between the initial d.d.t. temperature T_0 and the saturation temperature T_s. In most cases there is only a slight influence of superheating on the value of ψ_4 and for that reason we use as a rough approximation of T_v during the evaporation time τ

$$T_v = \tfrac{1}{2}(T_m + T_s) \tag{12}$$

where T_m is the time averaged d.d.t. temperature over the evaporation time.

The correction factor ψ_4 that would account for subcooling and superheating effects may be written as

$$\psi_4 = \left[\frac{\rho_d[H + \bar{c}_{dl}(T_s - T_d) + \bar{c}_{dv}(T_v - T_s)]}{\rho_{ds} H}\right]^{1/3} \tag{13}$$

where $\bar{c}_{dl}$ and $\bar{c}_{dv}$ are the mean specific heats of the liquid and the vapour of the droplet, while ρ_d and ρ_{ds} are the densities of the droplet at temperatures T_d and T_s. It is noted that equation (13) is based on the droplet radius, measured at the initial droplet temperature T_d with density ρ_d.

3.2. *Correction factor ψ_5 for droplet spattering*

In the analysis of Section 2 it is assumed that a droplet and all its liquid content stay in touch with the d.d.t. Spattering of the droplet at the moment of impact or during its evaporation would invalidate this assumption. The likelihood of the occurrence of spattering depends on many factors. It increases mainly with increasing droplet size and impingement velocity.

Furthermore, the rate of spattering during droplet evaporation increases with the initial d.d.t. temperature, especially for smooth d.d.t. surface.

The correction factor ψ_5 that accounts for spattering is less than or equal to unity, with the latter value corresponding to the case when no spattering occurs. Attempts have been made to establish the range of the validity of $\psi_5 = 1$ from measurements. Different parameters have been changed, such as impact velocity, initial d.d.t. temperature, droplet size and d.d.t. diameter. Some data are given in Section 4. In the presentation of these data the Weber number defined by (14) has been used.

$$W_e = \frac{2ru^2\rho_d}{\sigma} \tag{14}$$

where u is the impact velocity of the droplet and σ is the surface tension of the droplet.

3.3. *Correction factor ψ_6 for heat transfer from the surroundings to the droplet film*

If the droplet film receives some heat $Q_{\infty f}$ from the surroundings during its evaporation, the amount of heat Q_{cf} it draws from the d.d.t. decreases (see Fig. 5). The influence of this factor is estimated as

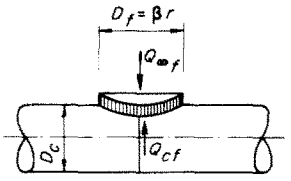

FIG. 5. Heat supply to droplet film on d.d.t.

follows. The droplet is at saturation temperature T_s. Approximating the contact area between droplet film and d.d.t. by the contact area between droplet film and surroundings, the heat transport ratio is written as

$$\frac{Q_{\infty f}}{Q_{cf}} = \frac{\alpha_{\infty f}(T_\infty - T_s)}{\alpha_{cf}(T_m - T_s)} \tag{15}$$

where $\alpha_{\infty f}$ is the heat-transfer coefficient from surroundings to droplet film;
α_{cf} is the heat-transfer coefficient from d.d.t. to droplet film;
T_∞ is the temperature of the surroundings.

Using (15), ψ_6 the correction factor for heat transfer from the surroundings to the droplet film can be written as

$$\psi_6 = \left[1 + \frac{\alpha_{\infty f}(T_\infty - T_s)}{\alpha_{cf}(T_m - T_s)}\right]^{-1/3} \tag{16}$$

Since heat removal from the d.d.t. is the leading effect for droplet evaporation we may approximate the value $\alpha_{cf}(T_m - T_s)$ in the following way

$$\frac{4}{3}\pi r^3 \rho_{ds} H = \frac{\pi}{4} D_f^2 \alpha_{cf}(T_m - T_s)\tau \tag{17}$$

with D_f the droplet film diameter.

Defining a ratio β as

$$\beta = \frac{D_f}{r}, \tag{18}$$

For droplet impact the value of β is in the order of 4, cf. [5] to [9] and the measurements described in Section 4. Substituting from (18) into (17) we get

$$\alpha_{cf}(T_m - T_s) = \frac{16rH\rho_{ds}}{3\beta^2\tau}. \tag{19}$$

The value $\alpha_{cf}(T_m - T_s)$ can be calculated from (19) using the values of r and τ found from the measured d.d.t. signal and an approximate value $\beta = 4$. On the other hand an upper limit value of the heat-transfer coefficient from the surroundings to the droplet film $\alpha_{\infty f}$ can be calculated ignoring the influence of the droplet film evaporation on this heat-transfer coefficient (like $\alpha_{\infty c}$ given in Section 3.4.). The value of $\alpha_{\infty f}$ increases at higher gas velocity and density but is nearly always very small in relation with α_{cf}.

Generally the value of ψ_6 is only slightly below unity and $\psi_6 = 1$ may be recommended as a reasonable approximation for general use.

3.4. *Correction factor ψ_7 for heat transport from surroundings to d.d.t.*

The temperature of a d.d.t. in surroundings at temperature T_∞, is always below T_∞ during droplet evaporation. This temperature difference between the surroundings and d.d.t. would cause a heat flow from the surroundings to d.d.t.

In particular for large droplets or high impact frequency, the time averaged d.d.t. temperature T_m decreases and consequently the driving temperature difference $(T_\infty - T_m)$ increases.

To approximate ψ_7 we compute the mean temperature rise $\theta_{\infty c}$ of the d.d.t. wires produced by the heat flow from the surroundings during the evaporation time τ. Let us assume that heat from the surroundings is supplied to both d.d.t. wires, each having length x and diameter D_c. Furthermore we assume perfect temperature equalization in the whole d.d.t. wire in calculating this temperature rise. Thus the heat flow from the surroundings to the d.d.t. wires during the evaporation time τ raises the d.d.t. temperature by an average of

$$\theta_{\infty c} = \frac{8\tau\alpha_{\infty c}(T_\infty - T_m)}{D_c(\rho_a c_a + \rho_b c_b)} \tag{20}$$

where $\alpha_{\infty c}$ is the heat-transfer coefficient from surroundings to the d.d.t. wires. Using heat-transfer literature [10] the value of $\alpha_{\infty c}$ can be calculated.

For a constant evaporation time τ the ratio between θ_c and $(\theta_c + \theta_{\infty c})$ yields the correction factor

$$\psi_7 = \left[1 + \frac{8\tau\alpha_{\infty c}(T_\infty - T_m)}{\theta_c D_c(\rho_a c_a + \rho_b c_b)}\right]^{-1/3}. \tag{21}$$

For the two wires a and b with perfect temperature equalization we can easily derive the time constant (to reach 63 per cent of the ΔT)

$$C_t = \frac{D_c(\rho_a c_a + \rho_b c_b)}{8\alpha_{\infty c}}. \tag{22}$$

Combination of (21) and (22) gives

$$\psi_7 = \left[1 + \frac{\tau(T_\infty - T_m)}{C_t\theta_c}\right]^{-1/3}. \tag{23}$$

Because of the small value of τ in comparison with C_t for small droplets, the value of ψ_7 is only slightly below unity in most practical cases. The value of ψ_7 decreases with the mean temperature difference $(T_m - T_s)$. This condition coincides with the increase of the evaporation time and the decrease of temperature drop (see Section 4.1., Table 1).

3.5. *Correction factor ψ_8 for time-dependent heat removal*

The assumption of constant heat flux q per unit time may not always be fully realized.

In general we may write $q = f(t)$ during heat removal from a d.d.t. (see Fig. 6).

Determination of the total temperature drop is possible using equation (1) and a simple addition or integrating process, if $q = f(t)$ is known and if the material properties k, ρ and c are independent of the temperature.

In case of n additive heat fluxes q_1 to q_n respectively, operating for times τ_1 to τ_n (at $x = 0$ and all ending at the same moment $t = \tau$), the total temperature drop at $t = \tau$ can be written as

$$\theta_{0\tau} = \sum_{i=1}^{n} \theta_{0\tau i} = \frac{2\sqrt{\kappa}}{k\sqrt{\pi}} \sum_{i=1}^{n} q_i\sqrt{\tau_i}. \tag{24}$$

For calculating ψ_8 we have to compare the process with constant heat flux q during time τ (process IA of Fig. 6) with the process $q = f(t)$. The comparison is done on the basis that both have the same integrated heat flux over the period τ. This yields

$$q\tau = \sum_{i=1}^{n} q_i\tau_i. \tag{25}$$

In case of a heat flux strongly decreasing with time (e.g. process $IIIA$ of Fig. 6) the measured cooling time τ_c (period between the moment $t = 0$ and the moment of maximum temperature drop θ_c) is shorter than the period of heat removal τ.

However, τ_c and θ_c are used for correlation with the droplet radius. For this reason we define

$$\psi_8 = \left[\frac{\theta_c\sqrt{\tau_c}}{\theta_{0\tau IA}\sqrt{\tau}}\right]^{1/3}. \tag{26}$$

For some special cases of heat flux vs time the value of ψ_8 is obtained from (26) (see Fig. 6). In case $IIIA$ the

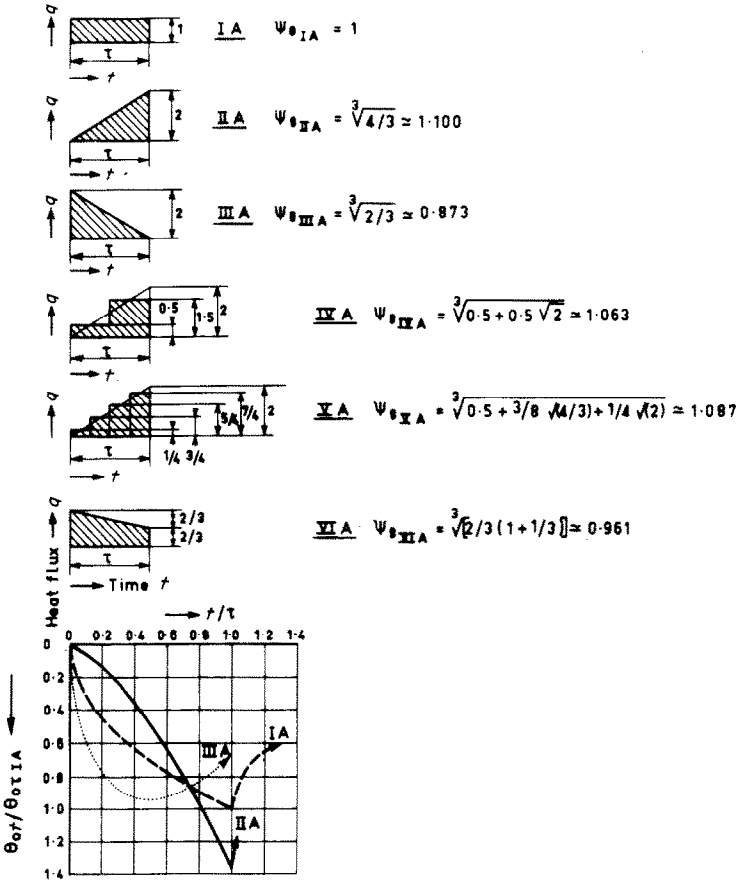

FIG. 6. Values of ψ_8 and signal shapes of some hypothetical $q = f(t)$.

maximum temperature drop θ_c occurs after a period $\tau_c = \frac{1}{2}\tau$. Consequently case *VIA* is a limit case with linearly decreasing heat flux vs time for which the cooling time τ_c equals the time of heat withdrawal τ.

From data given in Fig. 6 for some hypothetical extreme cases (*IIA* and *IIIA*) it is found that the value of ψ_8 differs only by about 12 per cent from unity, even in the case of strongly time-dependent heat fluxes. Moreover, we generally found during droplet detection that d.d.t. signal shapes were in fair agreement with the theoretical shape *IA* assuming constant heat flux.

For these reasons we conclude that a constant heat flux with $\psi_8 = 1$ is a reasonable approximation for most circumstances.

3.6. *Correction factor ψ_9 for heat removal beyond the junction*

In deriving the theoretical relation between droplet size and d.d.t. signal we assumed heat removal to occur only at the hot junction. However, a droplet evaporating at a distance x from the hot junction will give a d.d.t. signal depending on the value of x.

In order to calculate the value of the correction factor ψ_9 expressing this influence we assume constant and uniform material properties k, ρ and c for the entire d.d.t. wire. The temperature drop in an infinite wire at a distance x from the cross-section $x = 0$, from which continuous heat removal takes place, can be written as (see [2])

$$\theta_{xt} = \frac{q}{k}\left[\sqrt{\left(\frac{\kappa t}{\pi}\right)}e^{-x^2/4\kappa t} - \frac{|x|}{2}\operatorname{erfc}\frac{|x|}{2\sqrt{(\kappa t)}}\right] \quad (27)$$

with

$$\operatorname{erfc}\frac{|x|}{2\sqrt{(\kappa t)}} = 1 - \operatorname{erf}\frac{|x|}{2\sqrt{(\kappa t)}},$$

the complementary error function. Dividing (27) by the temperature drop θ_{0t} (at $x = 0$ and time t) we obtain a dimensionless temperature drop

$$\frac{\theta_{xt}}{\theta_{0t}} = e^{-x^2/4\kappa t} - \frac{|x|\sqrt{\pi}}{2\sqrt{(\kappa t)}}\operatorname{erfc}\frac{|x|}{2\sqrt{(\kappa t)}}. \quad (28)$$

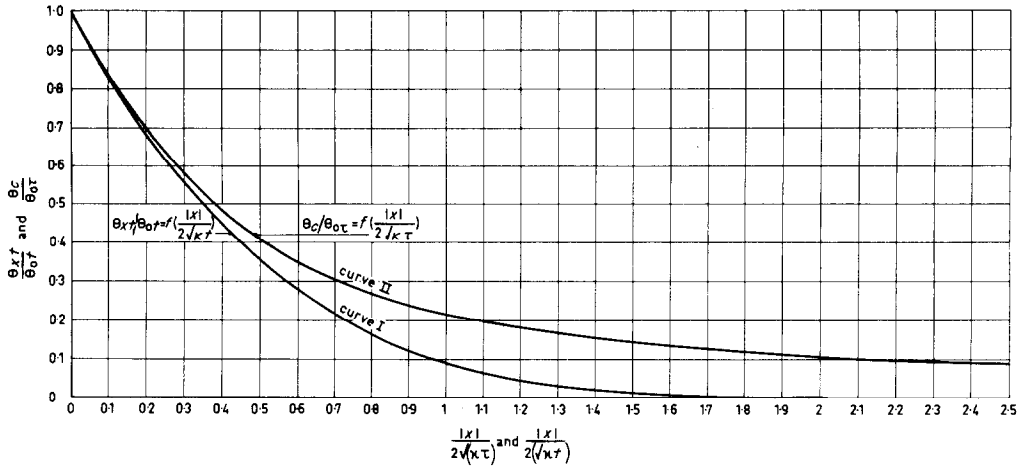

FIG. 7. Temperature drop ratios θ_{xt}/θ_{0t} and $\theta_c/\theta_{0\tau}$.

The relation (28), computed with values of the error functions from Abramowitz and Stegun [11], is plotted in Fig. 7 as curve I. With the temperature drop $\theta_{0\tau}$ (at $x = 0$ after a period τ) we obtain for continuous heat removal

$$\frac{\theta_{xt}}{\theta_{0\tau}} = \frac{\theta_{xt}}{\theta_{0t}}\sqrt{\left(\frac{t}{\tau}\right)}. \tag{29}$$

However, in case of droplet detection the constant heat flux q is only present during the evaporation time τ. This process can be built up by addition of two continuous processes with constant heat fluxes q and $-q$ respectively. The first of these represents a cooling process (with heat flux q) starting at the moment $t = 0$, the second a heating process (with heat flux $-q$) starting at the moment $t = \tau$. During evaporation we obtain from (29)

$$\frac{\theta_{xt}}{\theta_{0\tau}} = \frac{\theta_{xt}}{\theta_{0t}}\sqrt{\left(\frac{t}{\tau}\right)} \quad 0 \leqslant t \leqslant \tau. \tag{30}$$

After evaporation we obtain by superposition of the two processes, using (29)

$$\frac{\theta_{xt}}{\theta_{0\tau}} = \frac{\theta_{xt}}{\theta_{0t}}\sqrt{\left(\frac{t}{\tau}\right)} - \frac{\theta_{x(t-\tau)}}{\theta_{0(t-\tau)}}\sqrt{\left(\frac{t-\tau}{\tau}\right)} \quad t \geqslant \tau. \tag{31}$$

The shapes of the temperature signals, occurring at a distance x from the cross-section $x = 0$ (where heat is removed at a constant rate during period τ), can be calculated from (30) and (31).

For some values of $|x|/2\sqrt{(\kappa\tau)}$ the results are plotted in Fig. 8. For any value of $|x|/2\sqrt{(\kappa\tau)}$ a maximum

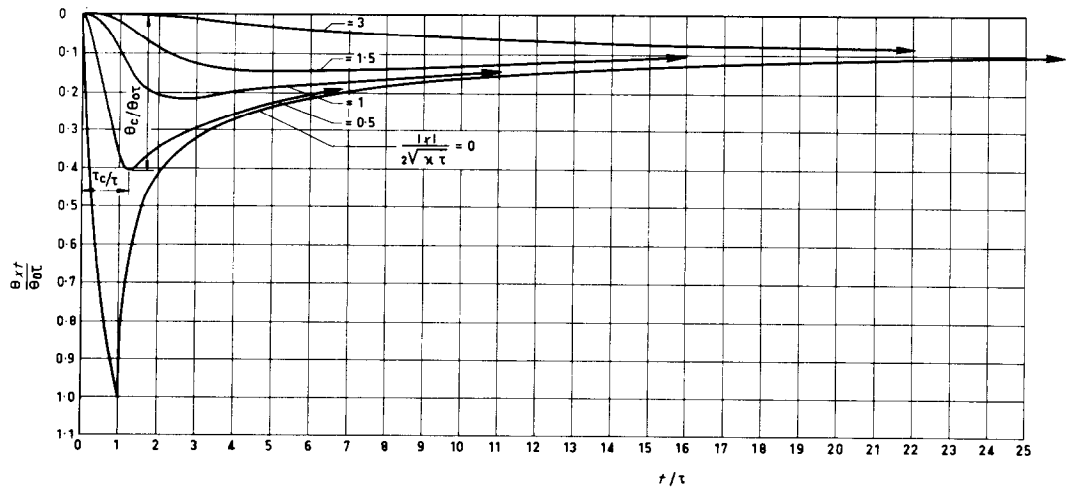

FIG. 8. Computed shapes of temperature signals at $x = 0$ resulting from constant heat removal during period τ at a distance x from the hot junction (equations (30) and (31)).

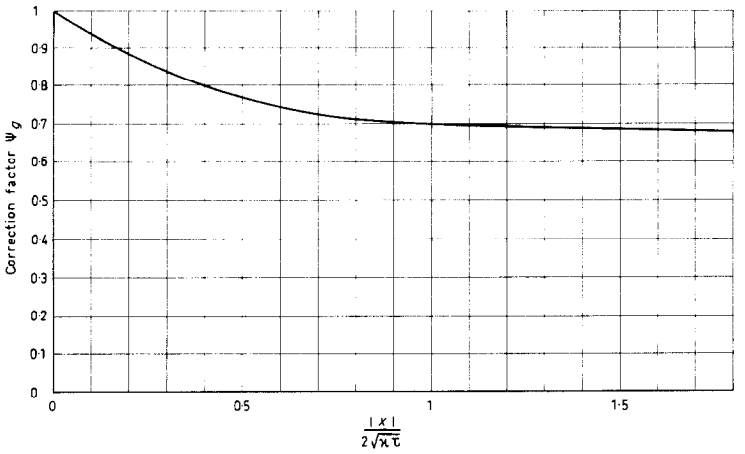

FIG. 9. Correction factor ψ_9 for heat removal at distance x from the hot junction.

value $\theta_c/\theta_{0\tau}$ of the dimensionless temperature drop exists, occurring at a time ratio τ_c/τ. As mentioned before the cooling time τ_c and the temperature drop θ_c are the correlating data used for droplet size measurement with d.d.ts. The value of $\theta_c/\theta_{0\tau}$ in relation with $|x|/2\sqrt{(\kappa\tau)}$ is given in Fig. 7 as curve II.

For droplets impinging at a distance x from the hot junction the correction factor ψ_9 has to be written as

$$\psi_9 = \left[\frac{\theta_c}{\theta_{0\tau}}\sqrt{\left(\frac{\tau_c}{\tau}\right)}\right]^{1/3}. \tag{32}$$

The relation between ψ_9 and $|x|/2\sqrt{(\kappa\tau)}$ is computed from (28), (31) and (32) and has been plotted in Fig. 9.

For large values of $|x|/2\sqrt{(\kappa\tau)}$ a lower limit value of ψ_9 exists (see [5])

$$\psi_9 = (4e)^{-1/6} \simeq 0{\cdot}67 \quad \text{if} \quad |x|/2\sqrt{(\kappa\tau)} \to \infty. \tag{33}$$

In general the value of x is not measured separately during droplet detection. However, the d.d.t. signal shape gives sufficient information about the value of $|x|/2\sqrt{(\kappa\tau)}$ for the determination of ψ_9.

3.7. *Correction factor ψ_{10} for finite droplet film diameter*

During the evaporation of a droplet on a d.d.t. surface a finite thermal contact area is present between droplet film and d.d.t. Consequently, heat removal from the d.d.t. always takes place over a finite axial distance in the neighbourhood of the hot junction. Evaluation of this influence is possible by calculating the correction factor ψ_{10} assuming constant and uniform material properties k, ρ and c for the entire d.d.t. wire.

We consider a droplet film with diameter D_f and its centre exactly at the hot junction ($x = 0$), as illustrated in Fig. 10. Assuming a constant and uniform heat flux

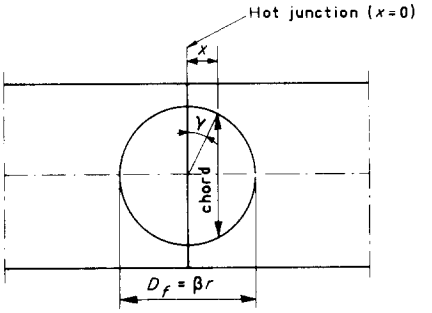

FIG. 10. Droplet film schematization for computing ψ_{10}.

q_f between droplet film and d.d.t. during the evaporation time τ we obtain

$$q_f = \frac{Qe}{(\pi/4)D_f^2\tau}. \tag{34}$$

The heat removal from a d.d.t. cross-section x is proportional with the chord $D_f \cos\gamma$ for $-\pi/2 \leqslant \gamma \leqslant \pi/2$. The angle γ is defined by $\sin\gamma = 2x/D_f$.

Assuming further that the heat removal by the droplet film at a distance x is uniform over the cross-section with area $(\pi/4)D_c^2$, the temperature drop in the hot junction ($x = 0$) will reach a maximum for $t = \tau$. The correction factor ψ_{10} for finite droplet film diameter may be derived in this case by integration:

$$\psi_{10} = \left[\int_0^{\frac{1}{2}D_f} \frac{\theta_{x\tau}\, 8\cos\gamma\, dx}{\theta_{0\tau}\pi D_f}\right]^{1/3}. \tag{35}$$

The results of the numerical integration in (35), using (28) at $t = \tau$, are plotted in Fig. 11.

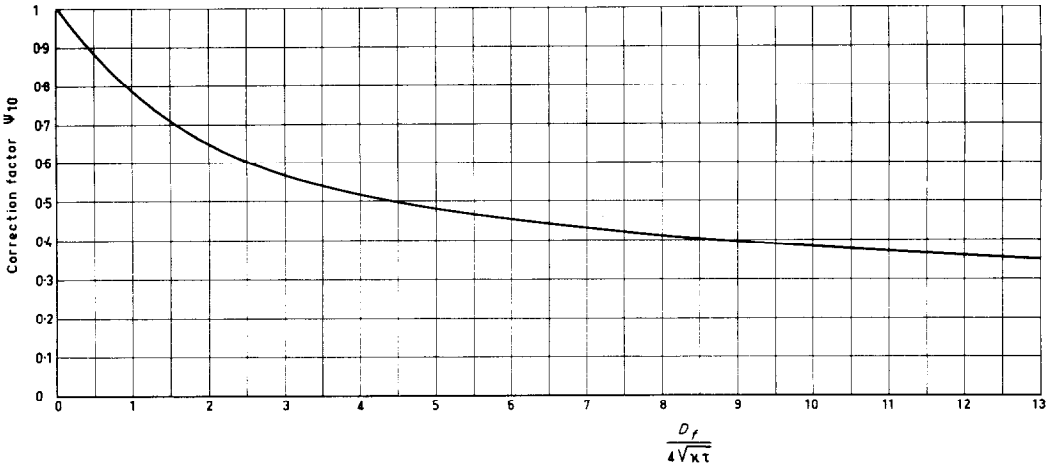

FIG. 11. Correction factor ψ_{10} for finite droplet film diameter.

For large values of $D_f/4\sqrt{(\kappa\tau)}$ there exists a asymptotic relation (see [5])

$$\psi_{10} = \left[\frac{4\sqrt{(\kappa\tau)}}{D_f\sqrt{\pi}}\right]^{1/3} \quad \text{if} \quad \frac{D_f}{4\sqrt{(\kappa\tau)}} \to \infty. \qquad (36)$$

For calculation of ψ_{10} the value D_f is often approximated as $D_f = 4r$, as mentioned in Section 3.4.

In most practical cases the value of $D_f/4\sqrt{(\kappa\tau)} \lesssim 1$, resulting in $0{\cdot}8 \lesssim \psi_{10} < 1$ during droplet measurement with a d.d.t.

3.8. *Correction factor ψ_{11} for non-uniform temperature across the hot junction*

With a simplified theoretical electrical analogon it can be proven that the temperature averaged over the cross-section of a hot junction is responsible for the measured e.m.f. This is obtained by assuming the e.m.f. of the hot junction to vary linearly with temperature and the electrical resistance of the thermocouple wires to be independent of temperature (see [5]). Using this result and assuming constant and uniform d.d.t. material properties k, ρ and c, it can be proven analytically that a constant heat flow Q_c/τ during time τ from any point of the hot junction will result in the same temperature signal as that obtained in case of a constant and uniform heat flux over the hot junction with the same heat flow Q_c/τ during the same time τ.

Moreover, in case of a relatively thin wire $[D_c/8\sqrt{(\kappa\tau)} \ll 1]$ the assumption of uniform heat flux over the cross-section of the hot junction is a reasonable approximation even in the case of different material properties k, ρ and c left and right from the hot junction (during normal droplet radius measurements with d.d.ts. it has been found that $0{\cdot}02 \lesssim D_c/8\sqrt{(\kappa\tau)} \lesssim 0{\cdot}2$.

For a bare chromel–alumel d.d.t. the aforementioned assumptions are reasonably correct, yielding $\psi_{11} = 1$ as a fair approximation.

3.9. *Sheathed d.d.ts.*

Bare thermocouples may fail under severe conditions (e.g. high temperatures or high pressures may result in defects in the glazing, cf. Fig. 1).

Sheathed thermocouples with mineral insulation (see Fig. 12) can be adapted for droplet detection. However, droplet measurement with sheathed d.d.ts. is less accurate than bare d.d.t. measurements. The main

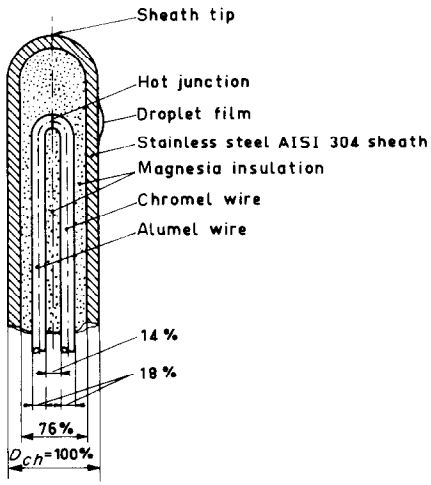

FIG. 12. Sheathed d.d.t. with droplet film at minimum distance from the hot junction.

reasons for this inaccuracy of sheathed d.d.ts. are:

(a) inaccurate mounting of the hot junction within the sheath;
(b) the variations in thermal conductivity of the mineral insulation;
(c) deviation of the actual conditions from those assumed in the following model.

A first calculation model for sheathed d.d.ts. is illustrated in Fig. 13 with the hot junction at $x = 0$.

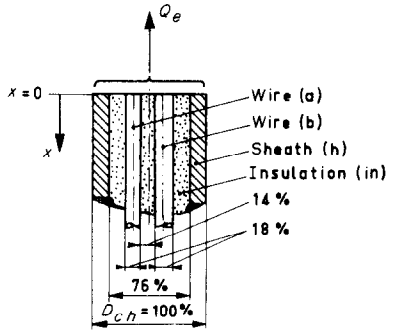

FIG. 13. Schematization of sheathed d.d.t. for heat flow analysis.

The assumptions of Section 2 hold, except for the sixth assumption. This assumption has been altered to the following: heat is withdrawn in an infinite slab at $x = 0$ with ideal radial temperature equalization and using mean values k_{ch} and $(\rho c)_{ch}$ for the axial heat transport defined by the following

$$k_{ch} = \frac{A_a k_a + A_b k_b + A_h k_h + A_{in} k_{in}}{A_a + A_b + A_h + A_{in}} \tag{37}$$

where A is the cross-sectional area of a material of the slab, while the subscripts (h) and (in) indicate the materials of sheath and insulation.

$$(\rho c)_{ch} = \frac{A_a \rho_a c_a + A_b \rho_b c_b + A_h \rho_h c_h + A_{in} \rho_{in} c_{in}}{A_a + A_b + A_h + A_{in}}. \tag{38}$$

In case of sheathed d.d.ts. and using the calculation model presented in Section 2, care should be taken that heat removal occurs only in one direction (in contrast with the model used for bare d.d.ts.). With this in mind, we obtain from an analysis similar to that of Section 2:

$$r^3 = C_{ch} \theta_{0\tau} \sqrt{\tau} \tag{39}$$

$$C_{ch} = \frac{3\sqrt{\pi D_{ch}^2 \sqrt{[k_{ch}(\rho c)_{ch}]}}}{32 H \rho_{ds}} \tag{40}$$

where D_{ch} is the outside diameter of the sheath.

Values of $\sqrt{[k_{ch}(\rho c)_{ch}]}$ are calculated for chromel–alumel thermocouples used (with magnesia insulation and sheathed with AISI 304 stainless steel and with dimensions as illustrated in Fig. 13). They were obtained assuming a magnesia density $\rho_{in} = 2120$ kg/m^3 and using thermal conductivity–temperature data for magnesia given by Deissler and Boegli in [12]. The results are plotted in Fig. 14. The correction factors for sheathed d.d.ts. may be derived using the analysis adopted for bare d.d.ts.

However, it is worth noting that for the influence of heat removal beyond the hot junction ψ_9, the large distance between the droplet film and the hot junction (in the order of $\frac{1}{2}D_{ch}$) results in large values of $|x|/2\sqrt{(\kappa\tau)}$, especially for low thermal conductivity of the insulation material. Thus the correction factor ψ_9 would have the value $\simeq 0{\cdot}67$ (see equation (33)) in case of sheathed d.d.ts. Furthermore a large value of $|x|/2\sqrt{(\kappa\tau)}$ coincides with $\tau_c/\tau \gg 1$, as can be seen in Fig. 8. This results in inaccurate values of ψ_7 when using equation (23), because τ (the period of heat removal by evaporation) becomes very small compared to τ_c (the registered cooling time of the signal) during which time heat supply from surroundings affects the important part of the d.d.t. signal.

On the other hand $\psi_{10} = 1$, seems a reasonable approximation for droplet measurement with sheathed d.d.ts. (cf. Fig. 12), due to the nearly uniform distance

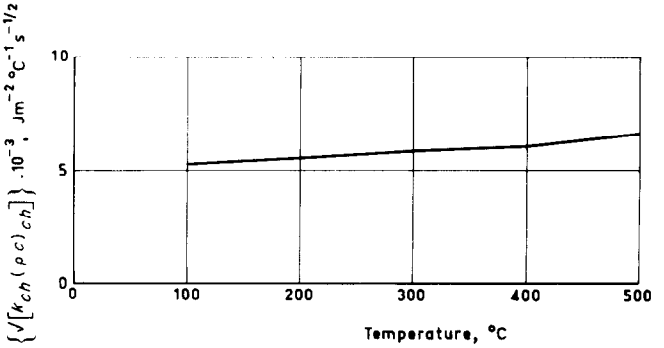

FIG. 14. Material factor $\sqrt{[k_{ch}(\rho c)_{ch}]}$ of stainless steel sheathed magnesia insulated chromel–alumel d.d.t. (see Section 3.9).

between the hot junction and the contact area of the droplet film with the d.d.t.

From radiographs of the sheathed d.d.ts. used, we may conclude that the distance between the tip of the sheath and the hot junction is in the order of D_{ch}. In case of a relatively large distance between this tip and hot junction (see Fig. 12) two-sided heat transfer becomes more realistic, resulting in a C_{ch} value twice as large as given by equation (40). However, the calibration factor ψ_w for sheathed d.d.ts. used in the following sections was calculated from equation (10), with r_j obtained from equations (39) and (40) (using τ_c and θ_c instead of τ and $\theta_{0\tau}$, resulting in $r_j^3 = C_{ch}\theta_c\sqrt{\tau_c}$) and the material factor given in Fig. 14.

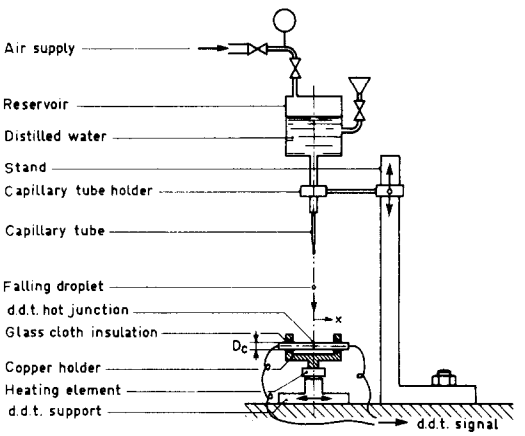

FIG. 15. Experimental set-up for large d.d.ts.

4. MEASUREMENTS

4.1. *Experiments with large d.d.ts.*

To evaluate the calculation model of Section 2 and the correction factors of Section 3, some experiments were devised and performed. To assure a high reproducibility and accuracy we used large droplets on large d.d.ts. at relatively low initial d.d.t. temperatures and small droplet impact velocities.

The experimental equipment used for droplet production and the d.d.t. measuring equipment are shown in Fig. 15. With reference to Fig. 15, heating of the copper holder is done electrically. Heat flows from the copper holder to the d.d.t. to heat the d.d.t. up to the desired level. The d.d.ts. used for the experiments presented in this section have been manufactured from chromel and alumel wires. These two wires were joined by a layer of hard solder (thickness about 0·05 mm). The sliding d.d.t. support permits changing the point of impingement on the d.d.t. surface. From the capillary tube (Fig. 15) uniform droplets impinge on the d.d.t. Changing the elevation of the capillary tube will cause a change in impact velocity. Droplet mass has been measured using a sensitive balance with a precision of 10^{-7} kg.

The relatively slow signals during the experiments were registered on a recorder (Kipp Micrograph B.D.5). Surrounding air and droplets leaving the capillary tube were at about the same temperature (between 22 and 25°C). The relative humidity of the surrounding air was in between 50 and 70 per cent. The evaporation time τ of a droplet was measured as the time between the moment of impact and the moment when the evaporating droplet film becomes invisible. In addition the axial distance x between the droplet film centre and the hot junction was measured during evaporation. (The value of x given in Table 1 is positive if the droplet film centre is situated on the chromel wire.) Data of the experiments are given in Table 1.

Table 1. Experiments with large d.d.ts.

D_c (mm)	r_w (μm)	T_0 (°C)	τ_c (s)	τ (s)	θ_c (°C)	u (m/s)	x (mm)	D_f (mm)	ψ_4	ψ_7	ψ_9	ψ_{10}	ψ_R	ψ_w	$\frac{\psi_w}{\psi_R}$	$\frac{D_c}{8\sqrt{(\kappa\tau)}}$
3·16	1142	124	16·8	18	21	0·5	0	2·5	1·060	0·921	1	0·982	0·959	0·947	0·987	0·042
3·16	1142	122	19·2	20	20·5	0·75	0	2·5	1·060	0·912	1	0·983	0·950	0·960	1·010	0·039
3·16	1150	98	40·8	—	13·75	0·75	0	2·5	1·057	0·841	1	0·990	0·880	0·916	1·041	0·027
3·16	1150	98	34·8	—	15·5	0·75	0	3·1	1·057	0·859	1	0·985	0·894	0·929	1·039	0·029
10·63	1182	112·7	7·3	—	3·75	1·27	0·5	4·5	1·060	0·994	0·980	0·952	0·983	0·990	1·007	0·212
10·63	1182	112	14	12	1·1	1·27	11·5	3	1·060	0·989	0·740	0·979	0·759	0·733	0·965	0·153
10·63	1188	101·5	18	19	2·38	1·27	0·5	3·5	1·058	0·985	0·988	0·978	1·007	0·974	0·967	0·135
10·63	1188	98·5	21	22	1·88	1·27	4	4	1·058	0·983	0·890	0·975	0·902	0·923	1·023	0·125
10·63	1188	112·4	15·6	—	1·62	1·27	7·5	3	1·060	0·987	0·800	0·980	0·820	0·845	1·030	0·145
10·63	1188	120·15	7	7	2·55	1·27	4	4	1·061	0·994	0·829	0·958	0·838	0·865	1·033	0·217
10·63	1188	123·6	7·5	6	1·38	1·27	11·5	4	1·061	0·994	0·705	0·960	0·714	0·713	0·999	0·209
10·63	1188	108·2	46	46	1·30	1·95	2·5	3	1·059	0·964	0·952	0·988	0·960	0·936	0·975	0·084
10·63	1184	112·8	15·6	15·2	2·65	1·95	0	4	1·060	0·987	1	0·972	1·017	0·999	0·982	0·145

The correction factor ψ_4 was calculated using equations (12) and (13) and values $T_d = 25°C$, $T_m = T_0 - \frac{1}{2}\theta_c$, $H = 2\,255\,500$ J/kg, $T_s = 100°C$, $\bar{c}_{dl} = 4180$ J/kg °C and $\bar{c}_{dv} = 2000$ J/kg °C. The droplet impact velocity u and the initial d.d.t. temperature T_0 were chosen in such a way that no visible spattering occurred, assuring the validity of the assumption $\psi_5 = 1$. For calculating ψ_6, the air temperature and velocity were measured in the neighbourhood of the droplet film, using a small 0·1 mm diameter bare chromel–alumel thermocouple. The air velocity was calculated using the measured time constant of this small thermocouple, equation (22) and convective heat transfer data from reference [10]. Using this calculated air velocity and data from [10] the value of α_{xf} on the top of the d.d.t. was calculated, assuming convection from air to the droplet film only. The calculated values of ψ_6 using these values α_{xf} and equations (16) and (19) are: $0{\cdot}998 \leqslant \psi_6 < 1$. This is the background for the assumption $\psi_6 = 1$ used in these experiments.

For computing ψ_7 the time constant C_t of the d.d.ts. was measured by briefly shielding the d.d.t. from the copper holder. The reheating process after unshielding yielded sufficient information about the values of C_t. In this manner values of $C_t = 35$ s and $C_t = 200$ s were found for d.d.ts. with diameters of 3·16 and 10·63 mm respectively. The correction factor ψ_7 was then calculated using equation (23) and approximating $(T_\infty - T_m) = \frac{1}{2}\theta_c$. For droplets impinging centrally on the hot junction ($x = 0$), the registered signal shapes conformed fairly well with the theoretical shape curve IA of Fig. 6. For that reason we conclude that a constant heat flux with $\psi_8 = 1$ is a reasonable approximation for the experiments reported here.

The correction factor ψ_9 is calculated using $\kappa = 5{\cdot}27 \times 10^{-6}$ m^2/s, this being the mean value of chromel–alumel between 100 and 300°C. As can be seen from Table 1 there is only a small difference between the cooling time τ_c (of the signal) and the evaporation time τ (measured by stop-watch). For this reason τ_c (instead of τ) has been used as a practical approximation for calculating the correction factors ψ_6, ψ_7, ψ_9 and ψ_{10}. Visual observations yielded the following conclusion: during the main time of droplet film evaporation a fairly constant droplet film area was present, only in the very last stage of evaporation a fast decrease of the film area has been observed. For this reason the correction factor ψ_{10} was calculated using the value D_f as given in Table 1, being the film dimension in axial d.d.t. direction as measured during the main time of droplet film evaporation. Mostly the film dimension in tangential d.d.t. direction (less important for ψ_{10}) was about 20 per cent larger than D_f given in Table 1 due to the impact on the round d.d.t. surface. Some important results of the experiments can be summarized as follows. Droplets centrally impinging on the hot junction (cf. Table 1 at $x = 0$) gave values: $\psi_w = 0{\cdot}916$ to $0{\cdot}999$. Hence we may conclude that the simple model given in Section 2 and resulting in equations (8) and (9) yields a reasonable approximation for droplet size measurement.

Moreover, the combined correction factor ψ_R calculated for the experimental measurements as $\psi_R = \psi_4\psi_7\psi_9\psi_{10}$ shows good agreement with the calibration factor ψ_w. The degree of agreement is shown in Table 1 by the ratio ψ_w/ψ_R being between 0·965 and 1·041.

The computed inaccuracies of ψ_w and ψ_R during the experiments are both in the order of $\pm 2{\cdot}5$ per cent and for this reason the 7·6 per cent spread found in ψ_w/ψ_R is acceptable.

Some of the experiences gleaned from the experiments are believed to be useful to the reader and are mentioned here. To prevent initial spattering of droplets with a radius $r = 1$–2 mm, a maximum Weber number of 100–130 is allowed (see equation (14)). To prevent spattering during evaporation of the droplet film, a maximum initial d.d.t. temperature of 125–130°C is allowable for droplets with radius $r = 1$–2 mm at room temperature. Sometimes a droplet impinging on the upper side of the d.d.t. slowly moves to a position on the lower side of the d.d.t. while still evaporating completely without spattering.

In case of large droplets and d.d.ts. and very high initial d.d.t. temperatures of 300–360°C the value of ψ_w decreases to about 0·2. In this case visible spattering occurs immediately after droplet impact on the d.d.t. surface.

The droplet film ratio $\beta = D_f/r$ increases with increasing values of droplet impact velocity, droplet radius and initial d.d.t. temperature.

4.2. *Calibration measurements using uniform droplets*

Small uniform droplets for d.d.t. calibration were produced with the aid of a vibrating capillary tube, as illustrated in Fig. 16. The capillary, reinforced by a piece of soft iron, was vibrated at one of its natural frequencies by means of a variable frequency electromagnet. The droplets leaving the vibrating capillary entered the surrounding air in chains. Under steady state conditions, each particular chain consists of uniform droplets. The number of chains and droplet radius in each chain depended on the water flow rate, the capillary frequency, the capillary diameter, etc. The droplets leaving the vibrating capillary showed a maximum radius of about 500 μm. The smallest droplets produced by this device were about 25 μm in radius and sometimes even smaller. However, the chains containing droplets with a radius $r \lesssim 25$ μm were only steady during a short time. Furthermore these

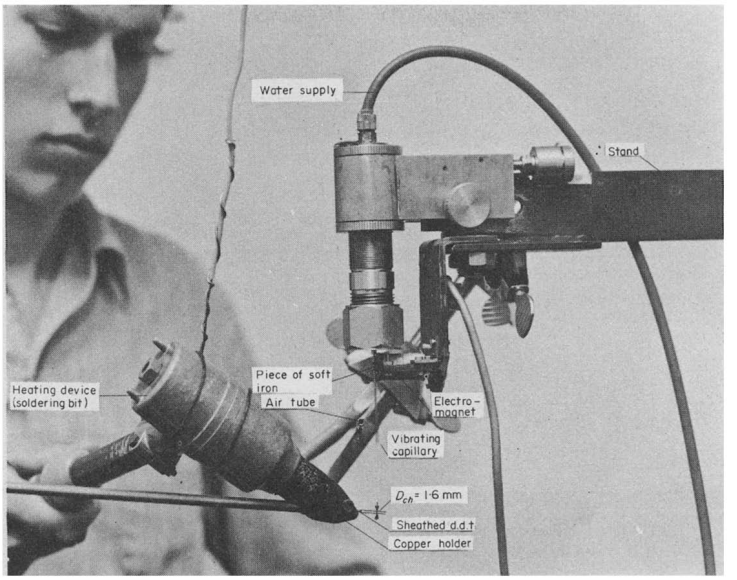

FIG. 16. View of vibrating capillary tube assembly used for d.d.t. calibration.

chains consisting of very small droplets were mostly interwoven with other chains consisting of larger droplets. For these two reasons the practical applicability of this calibration method is restricted to droplets of radius $\geqslant 25\,\mu$m. Droplets with a radius larger than $750\,\mu$m could be produced by collecting numerous small droplets (from the vibrating capillary) on a very fine wire tip. In this way the final droplet radius depended mainly on wire size.

Mostly an auxiliary air stream was used to produce some air turbulence, resulting in the enlargement of the distances between the droplets of a chain (the chain became more wide). In this way the droplet impact frequency on the d.d.t. could be regulated at the desired rate.

Measuring of the droplet radius was done by microscopic observation. For this purpose droplets of a particular chain were caught on glass slides in a layer of silicone oil (type Rhodorsil 47 V 100, viscosity 100 cS at 25°C). Small droplets with a radius $r \lesssim 40\,\mu$m were covered carefully with a second oil layer as illustrated in Fig. 17 to minimize evaporation prior to microscopic observation. Bare wire d.d.ts. (Fig. 1) and sheathed d.d.ts. (Fig. 12) were calibrated in ambient air.

Heating of the hot junction was done by an electrical heating element or by hot air. Control of the d.d.t. temperature took place electrically or by changing the position of the hot junction relative to the heating device. Moreover, another special d.d.t. (Fig. 18) was also used in calibration tests. For more difficult conditions this type has the advantage of permitting the

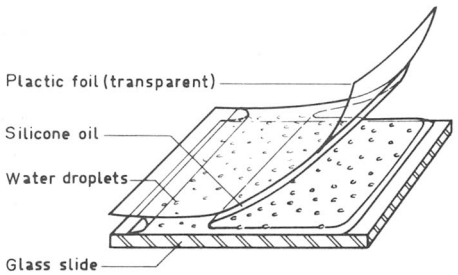

FIG. 17. Collection of droplets in silicone oil on a glass slide.

creation of a small region in the neighbourhood of the hot junction, with controlled conditions of temperature, gas velocity and gas composition. All the bare d.d.ts. used for calibration measurements were made of chromel and alumel wire. Their hot junctions were fabricated by electric arc welding for $D_c \leqslant 0{\cdot}15$ mm and by autogeneous welding for $0{\cdot}15\text{ mm} \leqslant D_c < 1$ mm.

The d.d.t. signals were registered on an oscilloscope (type Tektronix 564B Storage with differential amplifier 3A9 and time base 2B67). Some examples of signal shapes produced by uniform droplets with different values of $|x|/2\sqrt{(\kappa\tau)}$ are given in Fig. 19.

A calibration factor $\psi_w = 0{\cdot}98$ was found using equations (8)–(10) for the sharpest signal of this figure (with $\theta_c = 30{\cdot}7$°C, $\tau_c = 0{\cdot}006$ s, and starting point at 4·05 divisions before line A–A). Using (12) and (13), ψ_4 was found to be equal to 1·064. At the low impact velocity ($u \simeq 0{\cdot}5$ m/s) a value of 3 is estimated for β.

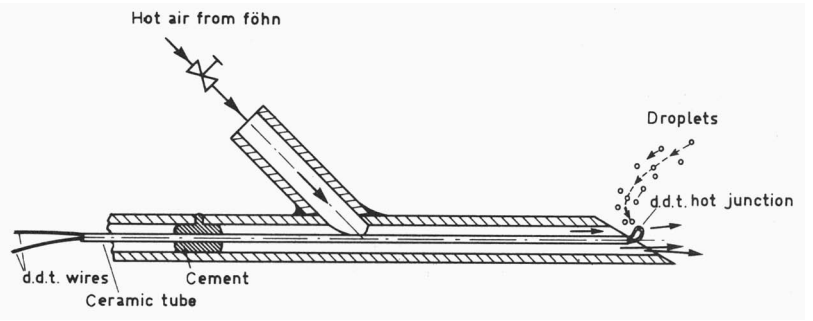

FIG. 18. Föhn d.d.t.

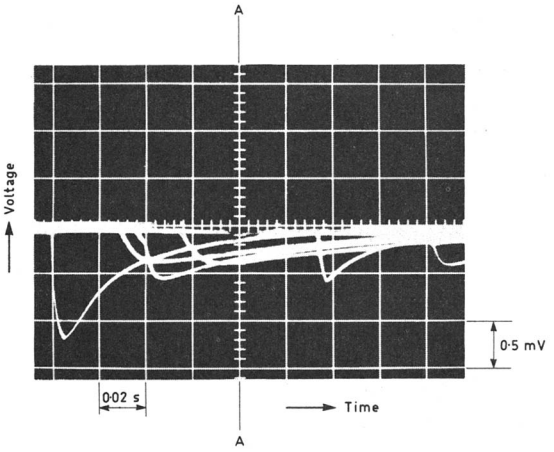

FIG. 19. Some d.d.t. signals produced by uniform droplets ($r_w = 75\,\mu$m, $T_d = 25°$C, $u \simeq 0{\cdot}5$ m/s) on a bare chromel–alumel d.d.t. ($D_c = 0{\cdot}33$ mm, $T_0 = 155°$C). Differences in shape are due to different impingement locations with reference to the hot junction, resulting in different values of $|x|/2\sqrt{(\kappa\tau)}$ and ψ_9.

Using $\kappa = 5{\cdot}27 \times 10^{-6}$ m^2/s, $D_f/4\sqrt{(\kappa\tau)}$ was calculated to be 0·316, resulting in $\psi_{10} = 0{\cdot}925$. Ignoring the small influences of other correction factors, we obtain $\psi_R = \psi_4\psi_{10} = 0{\cdot}985$, being in good agreement with the calibration factor found.

The unusual signal starting 2·2 divisions before line A–A is a combined signal, produced by two droplets. The time gap between the first and second droplet impact was about 0·01 s. The values $|x|/2\sqrt{(\kappa\tau)}$ for the first and the second droplet are in the order of 1 and 0·5 respectively, as may be deduced by comparing the combined signal with signal shapes of Fig. 8.

From numerous signals at low impact frequency it is statistically evident that the largest temperature drop has been produced by a droplet impinging at a minimum distance from the hot junction. This signal, referred to as "extremely sharp signal", has a maximum value of $\theta_c\sqrt{\tau_c}$. Extremely sharp signals have been used for calculation of the calibration factor ψ_w as found in Figs. 20–27. An extremely sharp signal of a bare d.d.t. would be produced by a droplet film with its centre at $x = 0$, resulting in $\psi_9 = 1$.

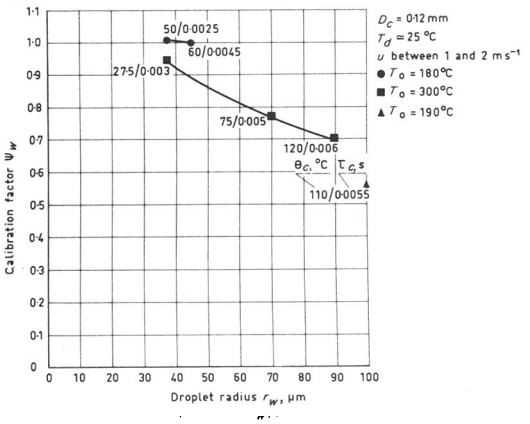

FIG. 20. Calibration factor of a 0·12 mm bare chromel–alumel d.d.t.

However, an extremely sharp signal of a sheathed d.d.t. would be produced by a droplet film at a minimum distance $x \simeq \frac{1}{2}D_c$ from the hot junction, mostly resulting in a value of $\psi_9 \simeq 0{\cdot}67$ (see Sections 3·6 and 3·9). The inaccuracy of r_w is about ± 5 per cent for droplets of $r \geqslant 40\,\mu$m and even somewhat larger for droplets with radius $15\,\mu\text{m} < r < 40\,\mu$m.

The value of the calibration factor found is in the order of 0·85 to 1·15 for bare d.d.ts. if the initial d.d.t. temperature is less than about 250°C and if the droplet radius yields $r \lesssim \frac{1}{2}D_c$ and $r \lesssim 140\,\mu$m. At higher initial d.d.t. temperatures or larger droplets, decreasing values of ψ_w have been found, probably caused by partial spattering off (see Figs. 20 and 21). However, it is worth mentioning that increased surface roughness and the presence of a thin layer of oxide or porous non-evaporating parts may result in complete droplet evaporation even at very high initial d.d.t. temperatures, especially for small droplets.

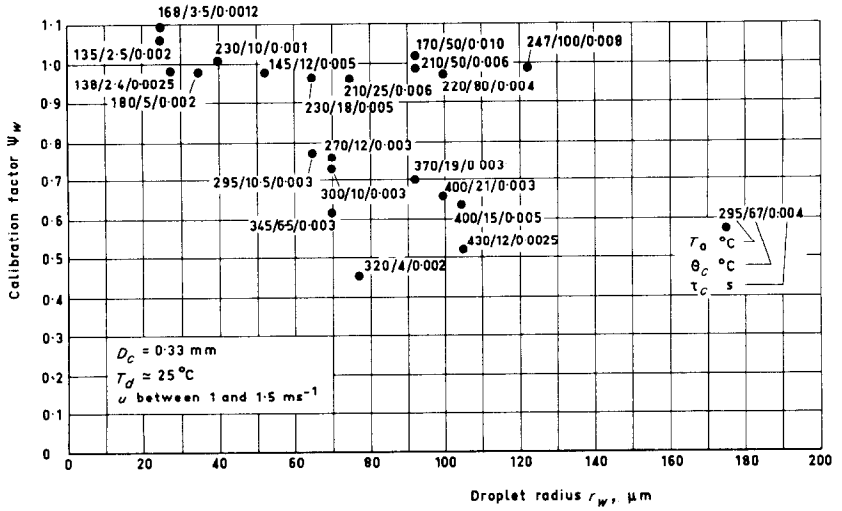

FIG. 21. Calibration factor of a 0·33 mm bare chromel–alumel d.d.t. for different initial d.d.t. temperatures.

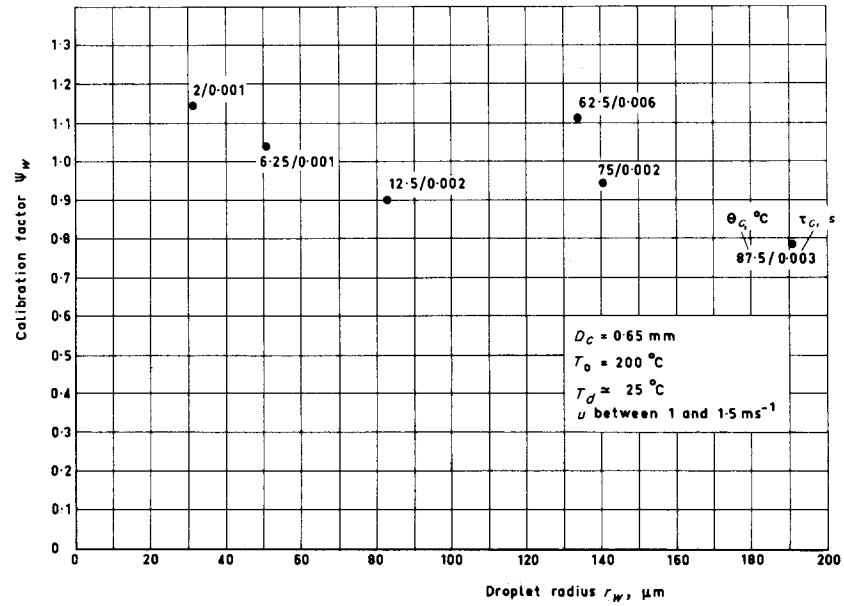

FIG. 22. Calibration factor of a 0·65 mm bare chromel–alumel d.d.t. with high surface roughness at $T_0 = 200°C$.

These relatively large values of ψ_w at very high initial d.d.t. temperatures were found using the 0·65 mm dia. bare d.d.t. with a comparatively high surface roughness, viz., in the order of 15 μm (see Figs. 23 and 24). Furthermore the ratio between droplet radius and d.d.t. diameter (r/D_c) is a limiting factor for accurate droplet measurement. A very small value of r/D_c (say $r/D_c < 0·05$) results in d.d.t. signals so small as to be nearly invisible on the scope screen. A very large value (of the order $r/D_c > 0·5$) often gives inaccurate droplet measurement due to excessive cooling of the d.d.t., resulting in a strongly decreasing heat removal with time. At moderate and high droplet impact velocities a value $r/D_c < 0·25$ is advisable to prevent spattering off during impact (because the droplet film diameter D_f is in the order of $4r$).

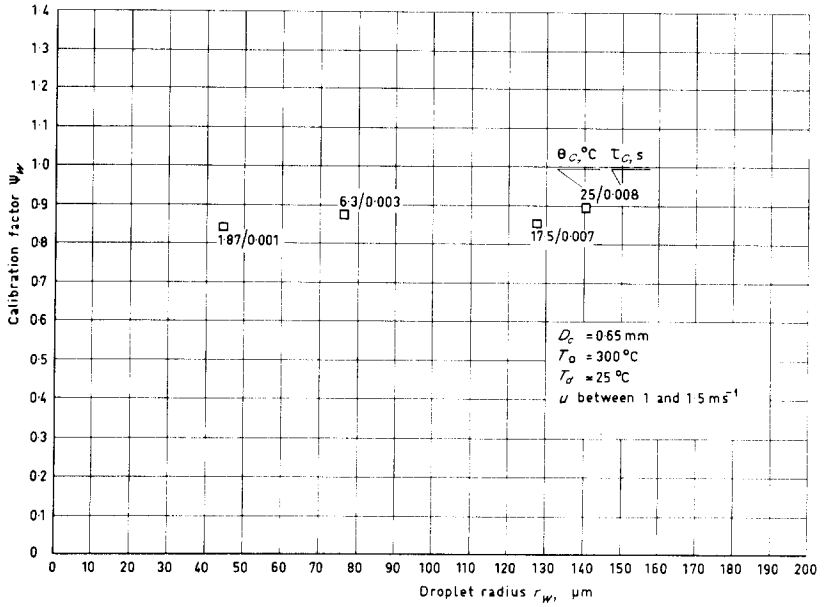

FIG. 23. Calibration factor of a 0·65 mm bare chromel–alumel d.d.t. with high surface roughness at $T_0 = 300°C$.

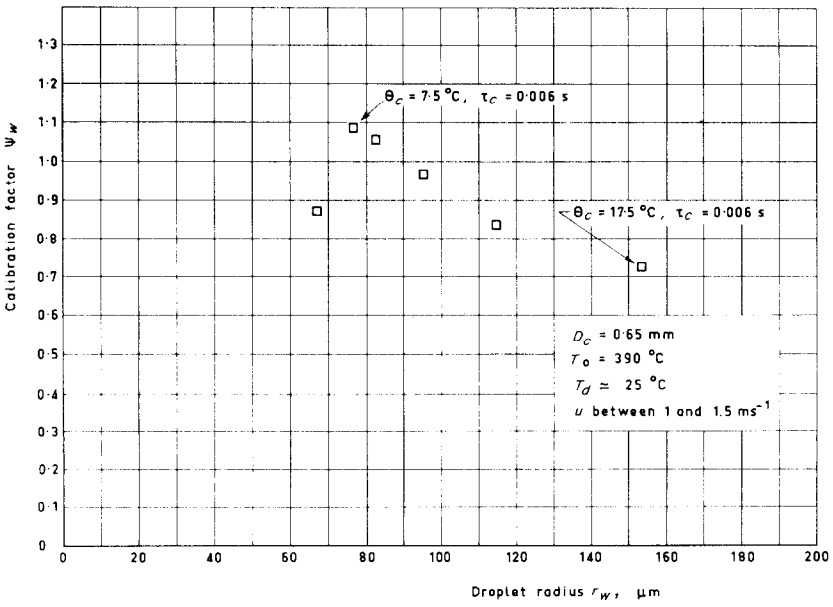

FIG. 24. Calibration factor of a 0·65 mm bare chromel–alumel d.d.t. with high surface roughness at $T_0 = 390°C$.

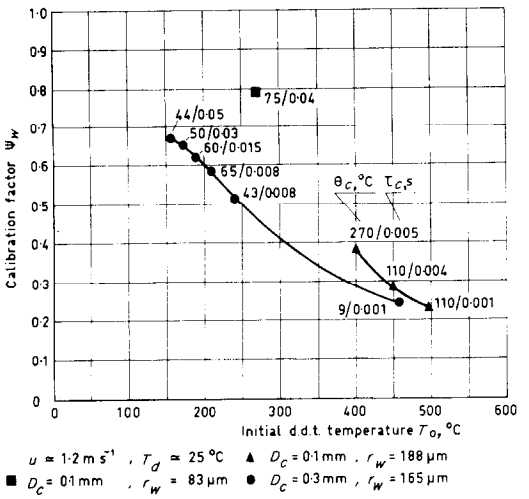

FIG. 25. Calibration factor of bare chromel–alumel d.d.ts. for different initial d.d.t. temperatures and relatively large droplets.

only the largest droplets, present in the outer side of the spray cone, have been used for calibration purposes. The radius of the largest droplet is measured by microscopic observation of numerous droplets on silicone oil covered glass slides (as was described in Section 4.2.). Care had to be taken to prevent excessive velocities of the droplets impinging upon silicone oil, in order to avoid droplets breaking up during capture. This dependence was separately investigated; the resulting data are presented in Fig. 28. The temperature and velocity history of the largest droplets may be calculated from their initial values, measured at the atomizer outlet, using literature data on flow resistance and heat transfer of droplets moving in air [1, 10] and assuming no air movement at the outer side of the spray cone. These computed droplet velocities agree with photographically measured droplet velocities, using the method described in [13]. The values of ψ_w were calculated using the largest droplet radius found by microscopic observation and using the d.d.t. signal with the largest value of $\theta_c\sqrt{\tau_c}$ (statistically caused by

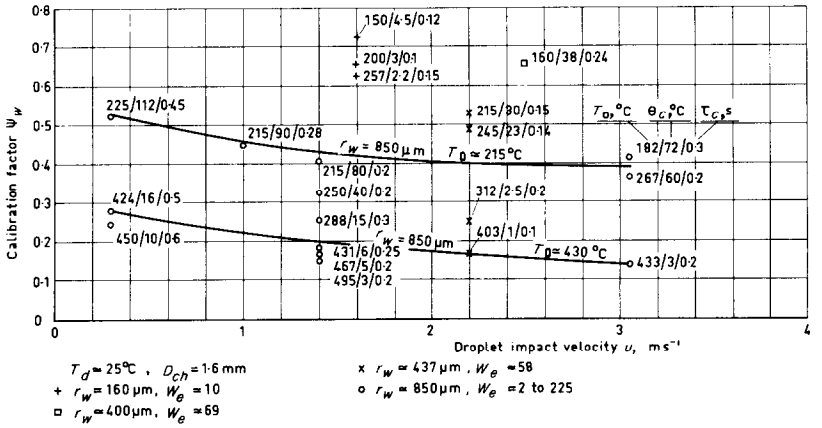

FIG. 26. Calibration factor of a 1·6 mm sheathed d.d.t. for different initial d.d.t. temperatures and impact velocities.

The mean value of the calibration factor for sheathed d.d.ts. is found to be about 0·7, if the initial d.d.t. temperature is less than about 250°C and $r \lesssim 200\,\mu m$ (cf. Figs. 26 and 27). This relatively small mean value is due to the small value of ψ_9 as indicated in Sections 3.6 and 3.9.

4.3. *Calibration measurements using droplets from swirl atomizers*

The influence of higher droplet impact velocities and higher droplet temperatures on the calibration factor has been measured, using droplets produced by swirl atomizers. However, droplets produced by swirl atomizers are non-uniform in size. For this reason one of the larger droplets impinging near the hot junction). The accuracy of these calibration measurements is limited, because the number of investigated droplets on glass slides and d.d.ts. was limited to a value in the order of 10^3 to 10^4 for one calibration condition. Some data on the calibration factor ψ_w at high impact velocity can be found in Figs. 29–31. Comparison of these data with data of Figs. 21–24 and 27 shows decreasing values of ψ_w for increasing impact velocities. For bare d.d.ts. this effect is at least partially caused by larger film diameters and shorter evaporation times at higher impact velocities. This results in increased values of $D_f/4\sqrt{(\kappa\tau)}$ coinciding with decreased values of ψ_{10}. Assuming $\beta = 4$ (as an estimated lower limit value at

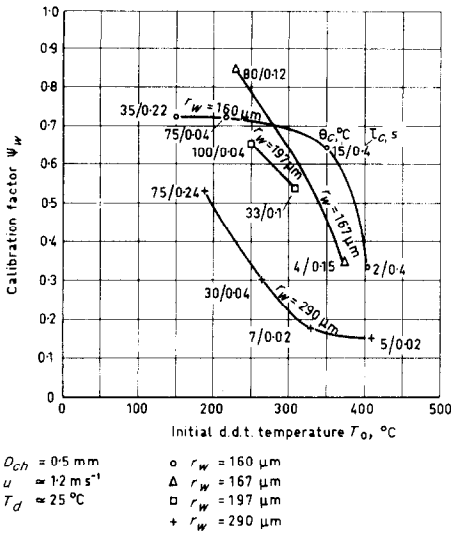

FIG. 27. Calibration factor of a 0·5 mm sheathed d.d.t. for different initial d.d.t. temperatures.

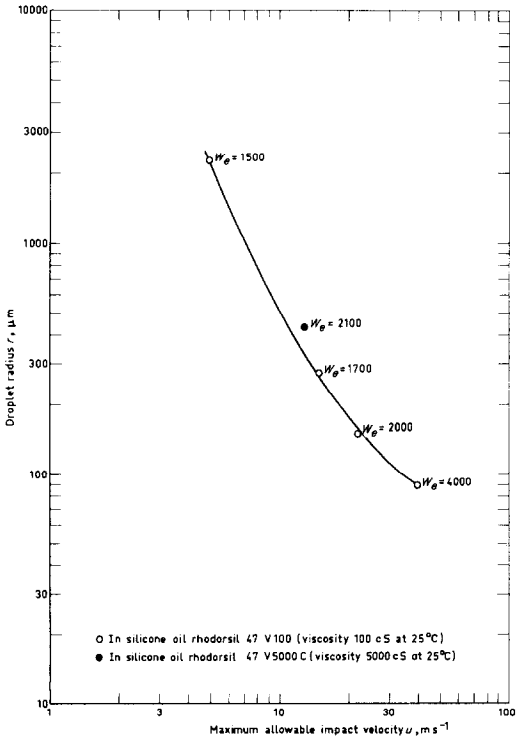

FIG. 28. Maximum allowable water droplet impact velocity on silicone oil at 25°C.

these conditions) some data of ψ_{10} are given in Fig. 30. For small droplets (radius 50–100 μm) at moderate initial d.d.t. temperatures (T_0 = 150–200°C) and high impact velocities (u = 16–40 m/s) resulting in high Weber number ($W_e \simeq$ 500–4000), the value of the calibration factor ψ_w still shows good agreement with the combined correction factor ψ_R (based on $\psi_5 \simeq 1$ and β = 4–6). Comparison of this result, with data of very large droplets (with radius r = 1–1·7 mm mentioned in Section 4.1. and given in more detail in [5]) shows a sharp increase in allowable Weber number and allowable initial d.d.t. temperature for decreasing droplet radius.

It is worth mentioning that the same order of allowable Weber number for small droplets ($r \simeq 80$ μm) was found for capture in silicone oil (see Fig. 28). Some experiments were performed with atomizer outlet water temperatures between 90 and 95°C, resulting in calculated droplet temperatures T_d between 70 and 80°C at impact on d.d.t., as shown in Fig. 30. Comparison of data of Fig. 30 shows little influence of the droplet temperature T_d on the calibration factor ψ_w.

4.4. *Calibration measurements using tiny droplets*

The need for accurate measurements of tiny droplets arises in several research and industrial applications (e.g. steam spray coolers, atomizers, droplet formation at condensation, etc.). When using the d.d.t. for measurements of tiny droplets the experimental evaluation of the calibration factor is rather difficult and time-consuming.

In our experiments droplets of radius $r \leqslant 25$ μm could be produced by a pneumatic atomizer as illustrated in Fig. 32. The atomization took place in ambient air at room temperature (22°C) and a relative humidity of about 60 per cent. The measurements described below were carried out using a water flow of $1{\cdot}7 \times 10^{-5}$ kg/s and atomizing air at a supply pressure of 5 bar (resulting in an air flow of about 2×10^{-4} kg/s). The droplet radii and d.d.t. signals were measured in the centre of the spray cone at a distance of 0·12 m below the atomizer. The measured spray velocity at that point was about 11 m/s. Using a bare chromel–alumel d.d.t. with D_c = 0·1 mm, as illustrated in Fig. 33, we found a d.d.t. signal distribution with a maximum signal of θ_c = 12·5°C, $\tau_c = 4 \times 10^{-4}$ s at an initial temperature T_0 = 170°C. Using glass slides, as illustrated in Fig. 17, the distribution of microscopically measured droplet radii r_{mi} was obtained. After impact of the droplets on the first silicone oil layer a period of about 3 s was needed to cover the droplets with the second oil layer. Mean values of the uncovered droplet evaporation Δr_e in a time span of 3 s were separately measured by microscopic observation and are shown in Fig. 34.

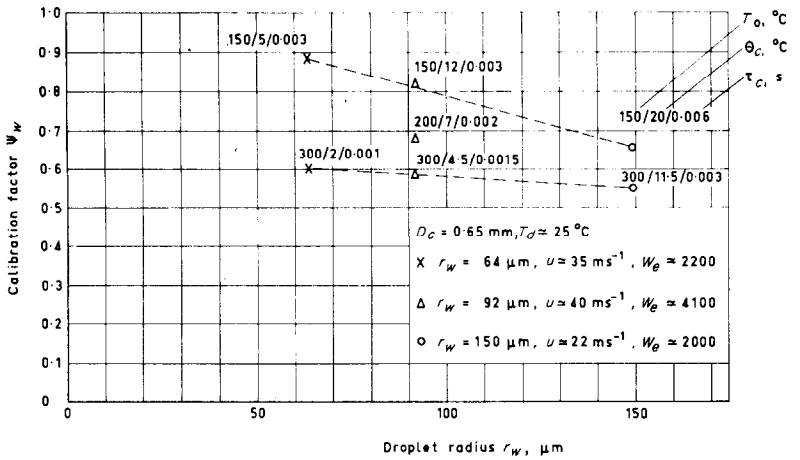

FIG. 29. Calibration factor of a 0·65 mm bare chromel–alumel d.d.t. with high surface roughness for high impact velocities.

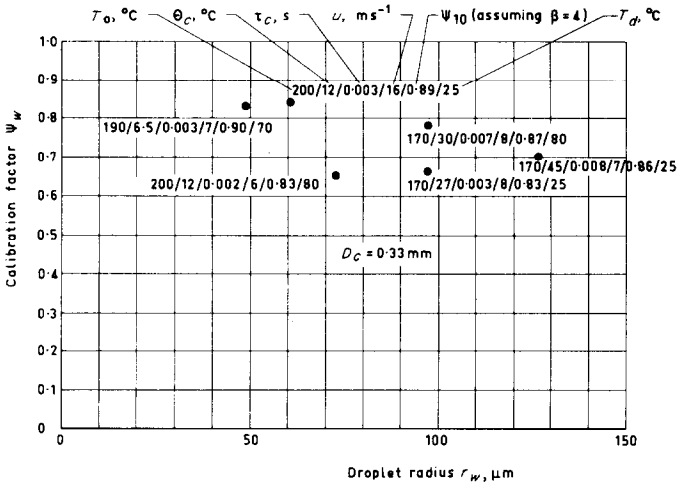

FIG. 30. Calibration factor of a 0·33 mm bare chromel–alumel d.d.t. for different impact velocities and droplet temperatures.

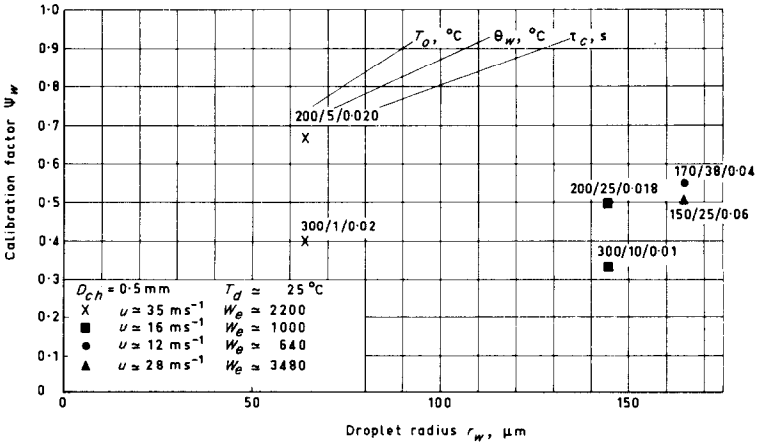

FIG. 31. Calibration factor of a 0·5 mm sheathed d.d.t. for different impact velocities and d.d.t. temperatures.

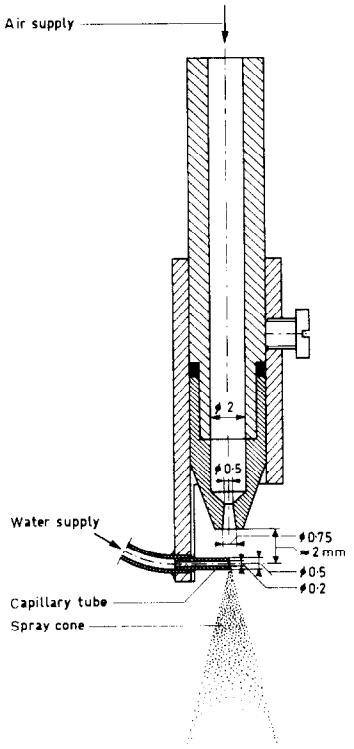

FIG. 32. Pneumatic atomizer.

on secondary influences. For this reason Δr_e is only significant for droplets of radius r_{mi} larger than about 5 μm. Microscopic observation of the droplets results in a droplet spectrum with a maximum value $r_{mi} = 15{\cdot}5$ μm corresponding to $r_w = 16\,\mu$m. Correlating $r_w = 16$ μm with the maximum d.d.t. signal found, yields $\psi_w = 0{\cdot}997$. Using (12) and (13), ψ_4 was found to be equal to 1·07. Assuming $\beta = 3{\cdot}5$ for these small droplets (Farlow and French [9] found $\beta = 3{\cdot}5$ at droplet radii between 5 and 40 μm even at high impact velocities) yields $\psi_{10} = 0{\cdot}93$. Approximating $\psi_5\psi_6\psi_7\psi_8\psi_9\psi_{11} = 1$ we find $\psi_R = 0{\cdot}995$, being in good agreement with the calibration factor ψ_w found.

Some further data about these measurements are worth mentioning: a maximum temperature drop of $\theta_c = 12{\cdot}5$°C was found during a recording time of 600 s on the oscilloscope. The droplet impact frequency on the d.d.t., visible by d.d.t. signals on the scope screen, was about 20 per second. The smallest signals observed showed $\theta_c = 0{\cdot}2$°C and $\tau_c = 10^{-4}$ s. Using $\psi_w = 1$ as a reasonable value for tiny droplets impinging the hot junction, we derive $r = 3\,\mu$m for these tiny signals. Assuming $\beta = 3{\cdot}5$ and using (19) we obtain $\alpha_{cf} \simeq 5 \times 10^5$ J/m^{2}s °C. A d.d.t. signal distribution was obtained in the same spray cone, using a criterion $|x|/2\sqrt{(\kappa\tau)} \leqslant 0{\cdot}5$ for the signals of this distribution.

Based on this signal distribution a new droplet

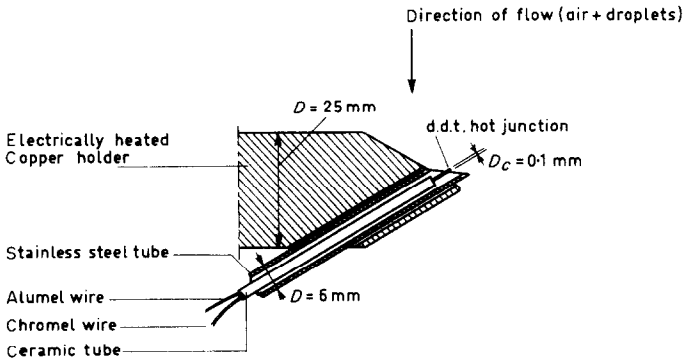

FIG. 33. Situation of d.d.t. within the electrically heated copper holder.

The droplet radius corrected for evaporation influences is calculated from

$$r_w = r_{mi} + \Delta r_e. \tag{41}$$

However, the droplet evaporation Δr_e for droplets of radius r_w smaller than about 7 μm, strongly depends

radius distribution was determined. This new droplet radius distribution showed good agreement with the droplet radius distribution r_w. In [5] additional information is given about these and other measurements of small and extremely small (airborne) droplets, together with some special applications of d.d.ts.

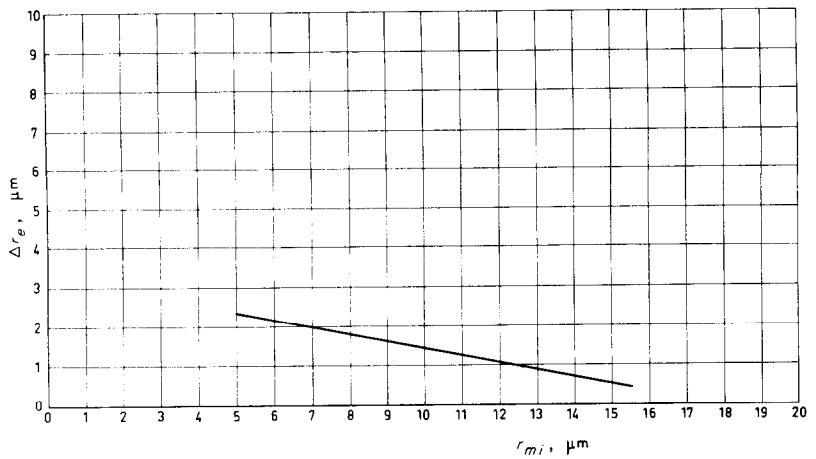

FIG. 34. Decrease in droplet radius over a period of 3 s Δr_e, vs droplet radius at the end of the same period r_{mi} (observed under the microscope).

5. CONCLUSION

D.d.ts. have proved to be practical devices for continuous measurement of large, small and tiny droplets. Using simple physical models, good correlation has been found between droplet radius and temperature signal.

The accuracy of droplet size measurement is high as long as droplet spattering at the d.d.t. is avoided. For water droplets of $r \lesssim 0{\cdot}1$ mm, allowable impact velocities as high as 40 m/s can be reached without the occurrence of spattering. The allowable droplet impact velocity and initial d.d.t. temperature increase with decreasing droplet radius and increasing roughness of the d.d.t.

As long as droplet spattering does not occur, d.d.t. calibration is often unnecessary, because the calculated value of the combined correction factor can be used as a calibration factor ($\psi_w \simeq \psi_R$). For bare d.d.ts. the calibration factor ψ_w is about unity if the droplet evaporates completely at the hot junction. For sheathed d.d.ts. the calibration factor ψ_w is about 0·7 if the droplet evaporates completely. The evaporation time of tiny droplets at the d.d.t. hot junction is in the order of 10^{-4} s, resulting in high allowable droplet detecting frequencies of 10^3 droplets per second. Droplet measurement in superheated steam or hot air may be done without any additional heating of the d.d.t. (Fig. 1). A Föhn d.d.t. (Fig. 18) has some advantages, especially for more difficult conditions. These advantages lie in the possibility of creating a small region in the neighbourhood of the hot junction, with controlled conditions of temperature, gas velocity and gas composition.

Acknowledgement—The assistance of the personnel of the Thermal Power Laboratory of the Delft University of Technology is gratefully acknowledged.

The author wishes to express his gratitude in particular to Prof. ir. J. J. C. van Lier, Prof. ir. D. G. H. Latzko, dr. H. H. Safwat, W. Klapwijk, A. D. van der Haar and C. A. C. M. van den Bergh for their valuable support.

REFERENCES

1. E. Giffen and A. Muraszew, *The Atomisation of Liquid Fuels*. Chapman and Hall, London (1953).
2. H. S. Carslaw and J. C. Jaeger, *Conduction of Heat in Solids*, 2nd Edn. Clarendon Press, Oxford (1959).
3. Hoskins Manufacturing Co., Chromel–Alumel thermocouple alloys, Catalog M-61 C-A, 7.5 A.P. 12/68, Detroit, Michigan (1961).
4. J. H. Perry, *Chemical Engineers Handbook*, 3rd Edn. McGraw-Hill, New York (1950).
5. C. A. A. van Paassen, Investigation of atomization- and evaporation processes using droplet detecting thermocouples (Dutch language), Thermal power laboratory of the Delft University of Technology, Internal report (September 1973).
6. C. O. Pedersen, An experimental study of the dynamic behavior and heat transfer characteristics of water droplets impinging upon a heated surface, *Int. J. Heat Mass Transfer* **13**, 369–381 (1970).
7. L. H. J. Wachters, The heat transfer from a hot wall to liquid drops in the spheroidal state (Dutch language), Diss. Delft (1965).
8. H. Rettig, Die Verdampfung von Tropfen an einer heissen Wand unter erhöhten Druck, Diss. Stuttgart (1966).
9. N. H. Farlow and F. A. French, Calibration of liquid aerosol collectors by droplets containing uniform size particles, *J. Colloid Sci.* **11**, 177–183 (1956).
10. Gröber, Erk and U. Grigull, *Die Grundgesetze der Wärmeübertragung*, 3rd Edn. Springer, Berlin (1955).
11. M. Abramowitz and I. A. Stegun, *Handbook of Mathematical Functions*. Dover, New York (1968).
12. R. G. Deissler and J. S. Boegli, An investigation of effective thermal conductivities of powders in various gases, *Trans. Am. Soc. Mech. Engrs*, 1417–1425 (1958).
13. C. A. A. van Paassen, Research on spray cooling (Dutch language), *Electrotechniek* **48**, 695–705, 745–754 (1970).

DETERMINATION THERMIQUE DE LA TAILLE DES GOUTTES PAR UN THERMOCOUPLE

Résumé—Au cours d'une étude de la pulvérisation et de l'évaporation d'eau dans des désurchauffeurs par injection, on a développé un instrument de mesure thermique pour la détermination de la taille des gouttes.

L'instrument consiste en un thermocouple sur lequel la goutte s'évapore par soutirage de la chaleur à la matière du couple, près de la soudure chaude.

L'instrument est appelé "droplet detecting thermocouple" (d.d.t.). Le principe d'un d.d.t. est basé sur l'utilisation de la corrélation entre la masse d'une goutte et le signal thermique du d.d.t. causé par l'évaporation de la goutte. Le d.d.t. parait être un instrument sûr pour détecter et mesurer en continu des gouttes d'eau, aussi bien dans un écoulement d'air que dans un écoulement de vapeur, même à haute pression et à température élevée.

Dans cet article on présente une analyse théorique du comportement du d.d.t. par rapport à des gouttes d'eau de rayon entre 3 et 1188 μm.

On montre que les résultats expérimentaux sont en bon accord avec l'analyse théorique.

THERMISCHE MESSUNG DER TROPFENGRÖSSE MIT EINEM THERMOELEMENT

Zusammenfassung—Zur Bestimmung der Tröpfchengröße während der Zerstäubung und Verdampfung von Wasser in einem Einspritzkühler zur Dampfkühlung wurde ein thermisches Meßinstrument entwickelt. Das Instrument besteht aus einem Thermoelement, auf dem Tropfen, die in die Nähe der heißen Lötstelle kommen, durch Wärmezufuhr vom Element verdampfen. Es wird mit "droplet detecting thermocouple (d.d.t.)" bezeichnet. Das Prinzip des d.d.t. beruht auf der Korrelation zwischen Tropfenradius und dem durch die Tropfenverdampfung ausgelösten Temperatursignal. Das d.d.t. hat sich als zur kontinuierlichen Anzeige und Messung von Wassertropfen sowohl in Luft- als auch in Dampfströmungen gut geeignet erwiesen. Es kann selbst bei hohen Drücken und Temperaturen eingesetzt werden. In diesem Aufsatz werden die theoretischen Grundlagen beschrieben und den experimentellen Ergebnissen für Wassertropfen mit Radien von 3 bis 1188 μm gegenübergestellt. Die berechneten und die experimentellen Werte zeigen gute Übereinstimmung.

ТЕПЛОВЫЕ ИЗМЕРЕНИЯ РАЗМЕРОВ КАПЛИ С ПОМОЩЬЮ ТЕРМОПАРЫ

Аннотация — При исследовании распыления и испарения воды в пароохладителе разработано тепловое измерительное устройство для определения размера капель. Это устройство состоит из термопары, на которой капля испаряется путём отвода тепла из материала термопары вблизи горячего спая, и названо каплеизмеряющей термопарой. Принцип каплеизмеряющей термопары основан на использовании корреляции между радиусом капли и температурным сигналом термопары, вызванным испарением капли. Каплеизмеряющая термопара оказалась надежным устройством для непрерывного выявления и измерения капель воды в струях воздуха и пара даже при высоких температурах и давлениях. В данной работе теоретический анализ поведения каплеизмеряющей термопары представлен вместе с экспериментальными данными для этих термопар при радиусах капель от 3 до 1188 мкм. Получено хорошее соответствие между экспериментальными данными и теоретическими расчетами.